Inorganic Chemistry

FORUM ARTICLE

pubs.acs.org/IC

Tale of a Twist: Magnetic and Optical Switching in Copper(II) Semiquinone Complexes

Pratik Verma, John Weir, Liviu Mirica, and T. Daniel P. Stack*

Department of Chemistry, Stanford University, Stanford, California 94305, United States

Supporting Information

ABSTRACT: An intermediate (**C**) that is observed in both phenol hydroxylation and catechol oxidation with the side-on peroxide species $[Cu_2O_2(DBED)_2]^{2+}$ (DBED = N^1,N^2-di-*tert*-butylethane-1,2-diamine) is identified as a copper(II) semiquinone species ($[\mathbf{1}]^+$) through independent synthesis and characterization. The reaction of the redox-active 3,5-di-*tert*-butylquinone ligand with $[(DBED)Cu^I(MeCN)]^+$ yields a copper(II) semiquinone $[\mathbf{1}]^+$ complex with a singlet ground state and an intense purple chromophore ($\varepsilon_{580} \sim 3500\ M^{-1}\ cm^{-1}$). All other copper(II) semiquinone complexes characterized to date are paramagnetic and weakly colored ($\varepsilon_{800} \sim 500\ M^{-1}\ cm^{-1}$). Antiferromagnetic coupling between the Cu^{II} center and the semiquinone radical in $[\mathbf{1}]^+$ is characterized by paramagnetic ^1H NMR and SQUID magnetometry. Comparative X-ray crystal structures along with density functional theory calculations correlate the geometric structures of copper(II) semiquinone complexes with their magnetic and optical properties. The unique observable properties of $[\mathbf{1}]^+$ originate from an increase in the overlap of the Cu 3d and semiquinone π orbitals resulting from a large rhombic distortion in the structure with a twist of 51°, attributable to the large isotropic demands of the *tert*-butyl substituents of the DBED ligand. Independent characterization of $[\mathbf{1}]^+$ allows the spectroscopic yields of intermediate **C** to be quantified in this intriguing hydroxylation reaction.

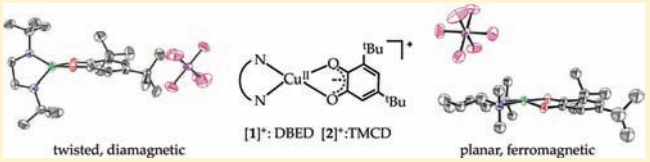

INTRODUCTION

Insight into the geometric and electronic structures of redox-active transition-metal ions with pro-radical ligands is valuable for the development of small-molecule systems that exploit ligand redox activity or "noninnocence" for catalytic applications.[1,2,3,1,4−8] Nature exploits the facile oxidation of hemes and phenolate ligands bonded to metals to create a radical-like species that serves as an electron acceptor in the catalytic reaction.[9,10] Distribution of the electron "holes" between the metal center and ligand is an intriguing strategy to potentially lower reaction barriers through lesser reorganization energy for two-electron substrate conversion reactions. Complexes of copper with pro-radical catecholate ligands and noninnocent semiquinone ligands have been identified as intermediates in catalytic oxidations of catechols by Cu_2O_2 and $Cu_2(OH)_2$ complexes.[11−17]

In a reaction reminiscent of enzyme tyrosinase, the μ-η^2:η^2-peroxodicopper(II) ($^S\mathbf{P}^{DBED}$) complex, formed by the oxygenation of $[(DBED)Cu^I(MeCN)]^+$ (DBED = N^1,N^2-di-*tert*-butylethane-1,2-diamine) at low temperatures, hydroxylates phenolate in reasonable yields (Figure 1).[18−20] The addition of phenolates to $^S\mathbf{P}^{DBED}$ at extreme temperatures (153 K) triggers a copper-core redox isomerization to a distinct phenolate-bonded bis(μ-oxo)dicopper(III) species (**A**). This intermediate, with limited stability even at 153 K, is best understood as the active electrophilic oxidant. The potential implications with respect to the viability of a Cu^{III} intermediate in a biological system is currently debated.[18,19,21] With 2,4-di-*tert*-butylphenolate (DBPHO) as the substrate, this intermediate species **A** decays rapidly at 173 K to a nearly colorless species (**B**), which can be transformed into a purple copper(II) semiquinone species (**C**) upon the addition of 1 equiv of acid. An acidic workup of the reaction mixture yields a 1:1 mixture of 3,5-di-*tert*-butylcatechol (DBCAT) and 3,5-di-*tert*-butylquinone (DBQ) upon decay.[18−20] The same intermediate **C** is also formed in a direct reaction of DBCAT with $^S\mathbf{P}^{DBED}$. While Cu_2O_2 cores are known to bind catechols to form thermally stable and air-stable copper(II) semiquinone complexes,[11,12] the intense purple chromophore of **C** is distinct from the pale green of all previously reported copper(II) semiquinone complexes.[12,16,22−24]

Herein is described the independent synthesis and characterization of the copper(II) 3,5-di-*tert*-butylsemiquinone complex of DBED ($[\mathbf{1}]^+$) and its one-electron-reduced congener, a copper(II) 3,5-di-*tert*-butylcatecholate complex (**1**). The intense ligand-to-metal charge-transfer (LMCT) band ($\varepsilon_{580} \sim 3500\ M^{-1}\ cm^{-1}$) of $[\mathbf{1}]^+$ correlates to its singlet ground state, which is distinct among all reported copper(II) semiquinone complexes. The significant rhombic distortion in $[\mathbf{1}]^+$ with a 51° twist from planarity is the origin of the unique optical and magnetic properties, highlighted through density functional theory (DFT) calculations and comparisons to the closely related $[(TMCD)Cu^{II}$(3,5-di-*tert*-butylsemiquinone)$]^+$ ($[\mathbf{2}]^+$; TMCD = N^1,N^1,N^2,N^2-tetramethylcyclohexane-1,2-diamine), a traditional, weakly colored ($\varepsilon_{800} \sim 500\ M^{-1}\ cm^{-1}$) copper(II) semiquinone complex with a triplet ground state.

Received: May 6, 2011
Published: June 22, 2011

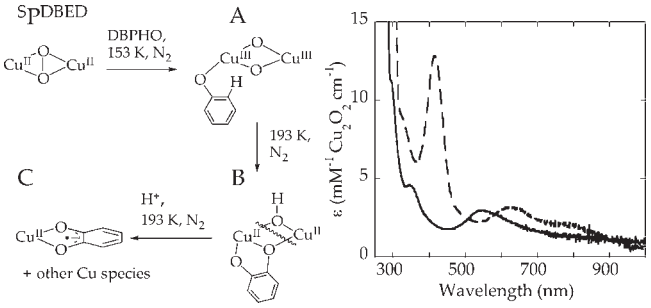

Figure 1. Phenolate hydroxylation scheme and UV−vis spectra of intermediates **A** (dashed) and **C** (solid).

Scheme 1. Copper(II) Catecholate and Copper(II) Semiquinone Complexes

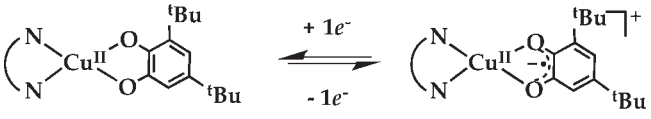

1: DBED **2**:TMCD [**1**]+: DBED [**2**]+:TMCD

RESULTS AND ANALYSIS

Synthesis and Crystal Structure Determination. The copper(II) catecholate complexes (**1** and **2**; Scheme 1) were synthesized readily from an internal-redox displacement reaction between the diamine (DBED and TMCD, respectively) and [Cu^{II}(3,5-di-*tert*-butylsemiquinone)$_2$] with the release of 1 equiv of DBQ.[25] The Cu^{II}(3,5-di-*tert*-butylsemiquinone) complexes ([**1**]$^+$ and [**2**]$^+$) were synthesized in a reaction of DBQ with [(DBED)Cu^{I}(MeCN)]$^+$ and [(TMCD)Cu^{I}(MeCN)]$^+$, respectively; the noncoordinating counteranions are varied readily by starting with appropriate [Cu^{I}(MeCN)$_4$]$^+$ precursors (SbF_6^-, PF_6^-, BF_4^-, and $CF_3SO_3^-$). **1** and [**1**]$^+$ are significantly more air-sensitive than **2** and [**2**]$^+$, decaying within minutes at room temperature. ORTEP plots of the crystal structures of **1**, [**1**]$^+$, and [**2**]$^+$ are shown in Figures 2 and 3, and selected metrical paramaters of the structures are collected in Table 1.[26] **1** crystallizes as a weakly associated, nonsymmetric dimer of two copper(II) catecholate monomers; one catecholate oxygen of each monomer bridges to the other copper center to create a Cu_2O_2 interaction (Figure S12 in the Supporting Information). The *tert*-butyl substituents of each DBED ligand are positioned cis to the N_2O_2Cu plane of each monomer, an atypical structural arrangement relative to the trans positioning observed in all other structures with the DBED ligand.[27]

Electrochemistry. Cyclic voltammograms of **1** and [**1**]$^+$ in CH_2Cl_2 at room temperature both contain two features (Table 2 and Figure S1 in the Supporting Information):[29] a reversible couple at ca. −570 mV (vs $Fc^{+/0}$) and a quasi-reversible oxidation at ca. +530 mV that remains irreversible even at 193 K. The former feature is a one-electron, diffusion-controlled process by comparison to the integrated charge of an equimolar $Fc^{+/0}$ standard (Table 2) and the linear response of the peak current with respect to the square root of the scan rate. The cathodic current in the differential pulse voltammetry measurement is much smaller than the anodic current, which further supports chemical rather than electrochemical irreversibility for the +530 mV feature.[29] The electrochemistry of **2** and [**2**]$^+$ is similar with several key differences relative to **1** and [**1**]$^+$. The reduction of **2** occurs at a more positive potential (ca. 90 mV), and the oxidation occurs at a less positive potential (ca. 170 mV) and is reversible.

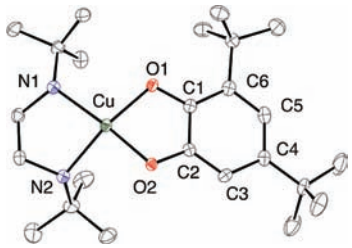

Figure 2. X-ray crystal structure of one of the copper(II) catecholate monomers in **1**.

Electron Paramagnetic Resonance (EPR) Spectroscopy. Frozen CH_2Cl_2 solutions of **1** and **2** both exhibit rhombic copper(II) EPR spectra at 77 K at the X band (Figures 4 and S2 in the Supporting Information and Table 2), consistent with a monomeric cupric species in solution.[29] While the copper hyperfine splitting (A_3) and g_3 parameters are within the range expected for N_2O_2 coordination for **1** and **2**, the ratio A_3/g_3 is smaller for **1**, consistent with a larger rhombic distortion (Table 3).[30,31] Frozen CH_2Cl_2 solutions of [**1**]$^+$ and [**2**]$^+$ were effectively EPR-silent (<5% signal relative to **1** and **2**) under all conditions examined ($\perp$ or $\parallel$ mode, X band or Q band, and 77 or 4 K), consistent with either a diamagnetic ground state or a triplet state with a large zero-field splitting.[16]

UV−Vis Spectroscopy. The electronic spectra of **1** and **2** contain intense features in the UV region (<300 nm and $\varepsilon >$ 8000 mM^{-1} cm^{-1}) consitent with $\pi \rightarrow \pi^*$ transitions associated with the catecholate aromatic ring and very low intensity features in the visible region (450 and 515 nm and $\varepsilon <$ 800 mM^{-1} cm^{-1}) attributed to Cu^{II} d−d bands and/or catecholate-to-copper charge-transfer transitions (LMCT; Figure 5). While the UV feature in **1** is less intense than the corresponding feature in **2**, the visible feature in **1** is lower in energy and more intense.

The electronic spectra of [**1**]$^+$ and [**2**]$^+$ contain intense features in the UV region (ca. 8000 and 14 000 mM^{-1} cm^{-1}, respectively) analogous to those of **1** and **2**, albeit at slightly lower energies (Table 4). In addition, the spectra of [**1**]$^+$ and [**2**]$^+$ contain additional intense features (ca. 2700 mM^{-1} cm^{-1}) in the near-UV region (350 and 380 nm, respectively) that are similar in energy and intensity to the 350 nm band observed in electrochemically generated free 3,5-di-*tert*-butylsemiquinone. This feature is attributable to a π-system transition within the semiquinone ligand and is not observed in free DBCAT.[23,33]

The electronic spectra of [**1**]$^+$ contains an intense broad feature in the visible region (580 nm and ∼3500 mM^{-1} cm^{-1}) that is absent in [**2**]$^+$; this broad band results in the characteristic purple color of [**1**]$^+$ that is absent in all previously reported copper(II) semiquinone complexes. At 193 K, this feature sharpens (ca. 5000 mM^{-1} cm^{-1}; Figure S3 in the Supporting Information).[29]

Resonance Raman (rR) Spectroscopy. Room temperature Raman spectra collected in resonance with the purple chromophore in [**1**]$^+$ (λ_{ex} ca. 530 nm) exhibits several diagnostic features (Figure 6). The 1372 cm^{-1} feature in the intraligand region, identical within experimental uncertainty to the feature in intermediate **C**, is diagnostic of metal-bonded semiquinones and attributed to C−O/ring mixed modes.[20] The three features in

dx.doi.org/10.1021/ic200958g |*Inorg. Chem.* 2011, 50, 9816–9825

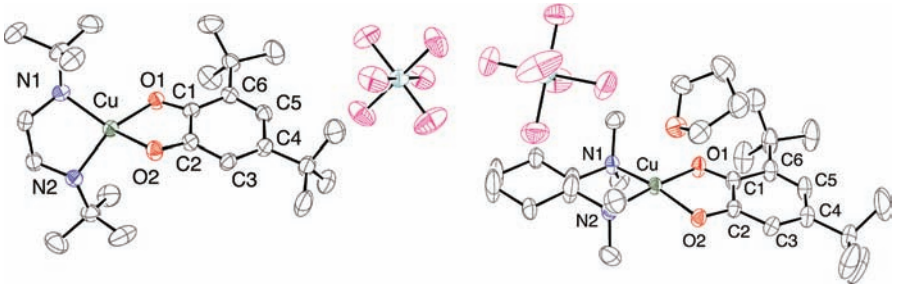

Figure 3. X-ray crystal structures of $[1]^+SbF_6^-$ (left) and $[2]^+SbF_6^-$ (right).

Table 1. Selected Experimental Metrical Parameters of the Structures of 1, $[1]^+$, and $[2]^+$

	1	$[1]^+$	$[2]^+$
Cu−O1	1.943(2)	1.975(2)	1.963(2)
Cu−O2	1.924(2)	1.924(2)	1.949(2)
Cu−N1	2.069(2)	2.002(2)	2.001(2)
Cu−N2	2.073(2)	1.993(2)	2.003(2)
twist ∠	18	51	14
τ_4[a]	0.2	0.5	0.1
O1−C1	1.347(3)	1.285(3)	1.289(3)
O2−C2	1.349(3)	1.269(3)	1.291(3)
C1−C2	1.425(4)	1.464(4)	1.455(4)
C2−C3	1.383(4)	1.421(4)	1.411(4)
C3−C4	1.411(4)	1.355(4)	1.370(4)
C4−C5	1.377(4)	1.448(4)	1.430(4)
C5−C6	1.409(4)	1.366(4)	1.367(4)
C6−C1	1.399(4)	1.441(4)	1.435(4)

[a] $\tau_4 = [360 - (\alpha + \beta)]/142$, where α and β are trans ∠N−Cu−O. Square planar: 0. Tetrahedral: 1.0.[28]

Table 2. Electrochemical Redox Potentials[a]

	E^1 [ΔE] (mV)	E^2 [ΔE] (mV)
1	−570 [130]	+520 [170][b]
2	−460 [100]	+350 [140]

[a] 0.1 M $TBAPF_6$, CH_2Cl_2, 50 mV s^{-1} at room temperature. ΔE for $Fc^{+/0}$ = 170 and 140 mV. [b] Irreversible.

the lower-energy region (502, 550, and 575 cm^{-1}), identical within experimental uncertainty to the three features in intermediate **C**, are attributed to Cu−L modes associated with the N_2O_2 coordination sphere.[20] An intraligand feature expected at ca. 1435 cm^{-1} is obscured by the solvent background.

Optical Redox Titrations of 1 and $[1]^+$. Because of the presence of intense features in the visible region, the interconversion of **1**/$[1]^+$ can be monitored readily using UV−vis spectroscopy. Titration of **1** with $Fc^{+/0}$ leads to a shift of the UV feature to lower energy and the appearance of features in the visible region at 350 and 585 nm that are associated with $[1]^+$ (Figures 7 and S4 in the Supporting Information). Full formation of $[1]^+$ requires ca. 1 equiv of Fc^+ and back-titration requires ca. 1 equiv of $CoCp_2$ (−1.33 V vs $Fc^{+/0}$) as monitored by the growth and decay of the 350 and 585 nm features in $[1]^+$. Corresponding titrations of synthesized $[1]^+$ with $CoCp_2$ and back-titrations with Fc^+ show similar behavior (Figure S4 in the Supporting Information).[29]

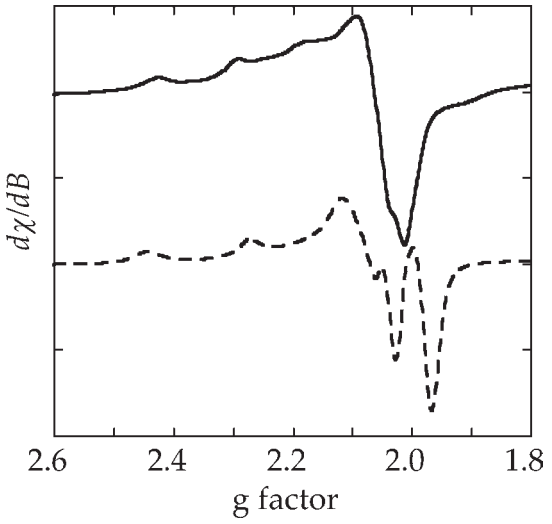

Figure 4. Frozen-solution X-band EPR spectra of **1** (solid) and **2** (dashed) (ca. 3 mM, CH_2Cl_2, 77 K).

Solid-State Magnetic Susceptibility. The solid-state magnetic susceptibility was measured for **1**, $[1]^+$, and $[2]^+$ using a SQUID magnetometer in the temperature range 5−300 K and four magnetic fields in the range of 0.1−0.8 T (Figure 8). In the solid state, $[1]^+$ is effectively diamagnetic and any residual signal can be attributed to <5% of a copper(II) impurity. The paramagnetic susceptibility of **1** and $[2]^+$ follows a linear dependence on $1/T$, and the magnetic moments, estimated from the Curie constants, are consistent with the spin-only values expected for $S = {}^1/_2$ (1.7 μ_B) and $S = 1$ (2.8 μ_B) systems, respectively.

Solution Magnetic Susceptibility. The bulk solution magnetic suceptibility was measured for **1**, $[1]^+$, and $[2]^+$ in the temperature range 220−300 K by Evans' method (Table 5).[34] Although the room temperature solution magnetic moments are slightly larger than those determined in the solid state, the same ground-state descriptions are applicable. The room temperature solution magnetic moments for **1** and **2** (2.0 and 1.8 μ_B, respectively) are consistent with the range of values (1.9−2.2 μ_B) observed for copper(II) complexes.[35] The value for $[1]^+$ (1.0 μ_B) is consistent with a diamagnetic ground-state description with minimal but measurable contributions from a paramagnetic species (vide infra), while the value for $[2]^+$ (2.7 μ_B) is consistent with two unpaired electrons in a triplet ground state.

^{1}H NMR Spectroscopy of $[1]^+$ and $[2]^+$. Similar to previously reported triplet ground-state copper(II) semiquinone complexes,[12] the room temperature ^{1}H NMR spectrum of $[2]^+$ exhibits

dx.doi.org/10.1021/ic200958g |*Inorg. Chem.* 2011, 50, 9816–9825

Table 3. Selected EPR Parameters[a]

	g_1	g_2	g_3	A_1	A_2	A_3
1	2.06	2.13	2.22	50	50	170
2	2.03	2.06	2.19	35	25	220

[a] Values are in units of G. Values are from a spectral fit using *EasySpin*.[32]

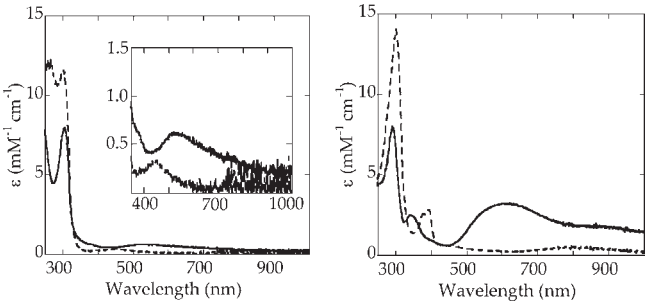

Figure 5. Solution UV−vis spectra of (left) **1** (solid) and **2** (dashed) and (right) $[\mathbf{1}]^+$ (solid) and $[\mathbf{2}]^+$ (dashed).

Table 4. Selected UV−Vis Parameters[a]

	λ_{max} (nm) [ε (mM^{-1} cm^{-1})]
1	300 [7900], 520 [600]
$[\mathbf{1}]^+$	290 [8000], 350 [2500], 600 [3200], 870 [1800]
2	260 [12 000], 300 [11 600], 450 [300]
$[\mathbf{2}]^+$	300 [14 000], 380 [2900], 450 [650], 800 [500]

[a] Measured at room temperature in CH_2Cl_2.

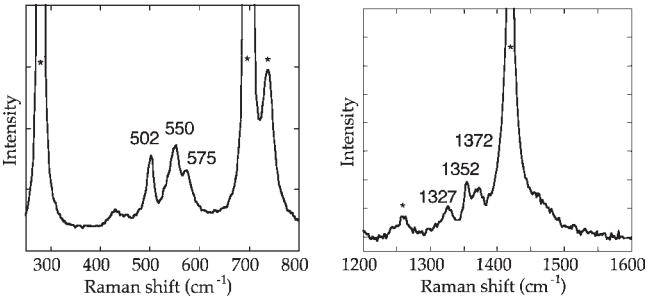

Figure 6. rR spectra of $[\mathbf{1}]^+$ (λ_{ex} = 530 nm, room temperature, CH_2Cl_2). Solvent features are marked with asterisks.

paramagnetically shifted resonances with broad linewidths (δ −6.7, −3.5, 4.1, 10.0, 27.3, and 28.8), but the majority of the resonances are resolved. Compared with $[\mathbf{2}]^+$, fewer ^{1}H NMR resonances with broader linewidths are observed for **1** and **2**. The ^{1}H NMR spectrum of $[\mathbf{1}]^+$ exhibits relatively narrow resonances within a limited spectral window (−2 to 10 ppm) that sharpen upon cooling (Figure 9). All of the peaks of the complex could be assigned.[29] While the change in the bulk solution magnetic susceptibility with the temperature is small as assessed by Evans' method, the chemical shifts of individual ^{1}H NMR resonances of $[\mathbf{1}]^+$ exhibit a reversible and quantifiable dependence on the temperature that can be modeled with contributions from a thermally populated triplet state with eq S1 in the Supporting

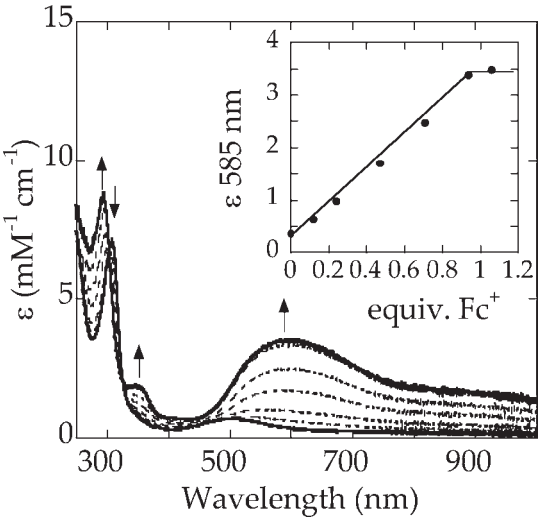

Figure 7. Redox titration of **1** with Fc^+ in CH_2Cl_2 at room temperature (inset: increase in the 585 nm intensity with equivalents of Fc^+).

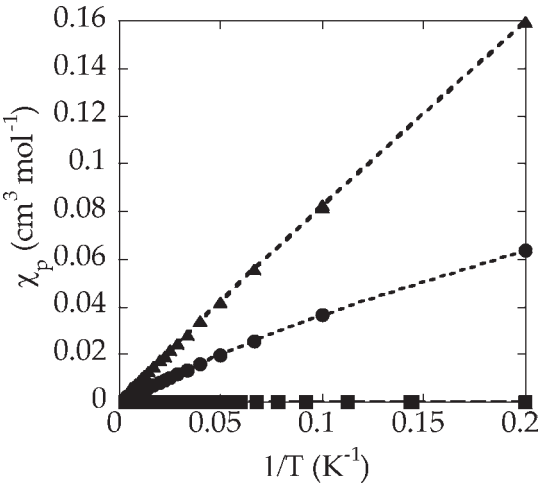

Figure 8. Curie plots for **1** (circles, C = 0.33 cm^3 mol^{-1} K, 1.62 μ_B), $[\mathbf{1}]^+$ (squares), and $[\mathbf{2}]^+$ (triangles, C = 0.80 cm^3 mol^{-1} K, 2.53 μ_B) collected at 0.1, 0.3, 0.6, and 0.8 T.

Table 5. Solution Magnetic Susceptibility[a]

	χ_p (10^{-3} cm^3 mol^{-1})	χ_pT (cm^3 mol^{-1} K)	μ_{eff}
1	1.71	0.514	2.02
$[\mathbf{1}]^+$	0.44	0.132	1.00
2	1.41	0.420	1.83
$[\mathbf{2}]^+$	3.17	0.950	2.75

[a] Measured in CD_2Cl_2 using Evans' method at 7.05 T (300 MHz).

Information.[36] Simultaneous fitting of the temperature dependence of all ^{1}H NMR resonances to a single value of the singlet−triplet energy gap yields a value of ca. 2300 cm^{-1}. The changes in the chemical shifts of the most sensitive ^{1}H NMR resonances in $[\mathbf{1}]^+$ are much smaller than those observed in other antiferromagnetic complexes with a smaller singlet−triplet gap.[37]

Theoretical Calculations. DFT geometry optimizations of $[\mathbf{1}]^+$ and $[\mathbf{2}]^+$ reproduce the experimentally observed quinoid pattern in the aromatic ring bond lengths and the large and small

dx.doi.org/10.1021/ic200958g |*Inorg. Chem.* 2011, 50, 9816–9825

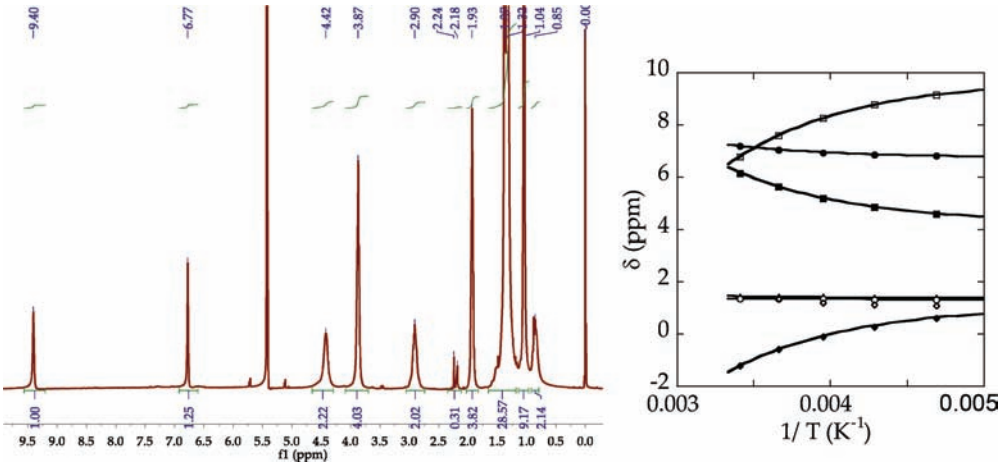

Figure 9. Low-temperature (193 K) ^{1}H NMR spectra (left) and a ^{1}H NMR derived Curie plot (right) for $[\mathbf{1}]^+$ (CD_2Cl_2, 12 mM).

Table 6. Selected DFT-Computed Metrical Parameters of Copper(I) Quinone and Copper(II) Semiquinone Electronic States for the DBED and TMCD Ligands[a]

		copper(II) semiquinone/DBED		copper(II) semiquinone/TMCD	
	copper(I) quinone/DBED	$S = 0$	$S = 1$	$S = 0$	$S = 1$
Cu−O1	1.991	1.939	1.925	1.925	1.924
Cu−O2	1.967	1.909	1.904	1.907	1.906
Cu−N1	2.004	2.007	2.016	2.002	2.008
Cu−N2	2.007	2.026	2.042	2.003	2.008
O1−C1	1.268	1.297	1.304	1.302	1.304
O2−C2	1.270	1.301	1.307	1.303	1.304
C1−C2	1.494	1.470	1.463	1.466	1.464
C2−C3	1.422	1.410	1.408	1.409	1.408
C3−C4	1.372	1.381	1.382	1.381	1.382
C4−C5	1.458	1.445	1.443	1.444	1.443
C5−C6	1.372	1.379	1.381	1.381	1.381
C6−C1	1.448	1.438	1.435	1.435	1.435

[a] The numbering scheme is from Scheme 2.

rhombic distortions in the copper coordination spheres {$[\mathbf{1}]^+$ exp (calc): 51° (50°); $[\mathbf{2}]^+$ exp (calc): 14° (17°); Table 6}. The antiferromagnetic ground state of $[\mathbf{1}]^+$ needs to be modeled within a broken-symmetry singlet formalism as the unrestricted calculations converge to a restricted solution best described as copper(I) quinone (Table 6). Including electronic energies and thermal corrections using a hybrid functional, the broken-symmetry solution for $[\mathbf{1}]^+$ is stabilized by ca. 5 kcal mol^{-1} relative to the triplet state and by 9 kcal mol^{-1} relative to the diamagnetic copper(I) quinone state.[29] For the less twisted $[\mathbf{2}]^+$, the broken-symmetry solution is stabilized relative to the triplet state by ca. 1 kcal mol^{-1}. For the broken-symmetry electronic state for $[\mathbf{1}]^+$, the α singly unoccupied molecular orbital (α-SUMO) is localized on the Cu 3d-centered and O- and N-centered orbitals involved in σ bonding to the metal, while the β-SUMO is predominantly localized on a π orbital of the semiquinone ring (Figure 10). While the spin of both the SUMOs is the same in $[\mathbf{2}]^+$, the qualitative character of the two SUMOs is similar to that of $[\mathbf{1}]^+$.

DFT computations of the singlet and triplet electronic states for a series of rhombically distorted monocationic copper(II) complexes using ethylenediamine and semiquinone as ligands are particularly insightful for understanding the magnetic properties of these complexes (Figures 11 and 12, Scheme 2, and Table 7). For a planar structure, the triplet electronic state is energetically favored by ca. 1 kcal mol^{-1}. With increasing rhombic distortion, controlled by partial geometric optimization with fixed N−Cu−N/O−Cu−O plane intersection angles, the triplet state is destabilized and the broken-symmetry state is stabilized; the crossover point occurs at ca. 20°, where the singlet state becomes energetically favored. The increasing overlap between the SOMOs (the α and β in the broken-symmetry state and the α in the triplet state) leads to stabilization of the broken-symmetry state due to improved bonding and destabilization of the triplet state due to the Pauli replusion between like-spin pairs. Notably, DFT computations predict that the planar triplet structure is the lowest-energy structure in the series.

For a planar structure, the copper(I) quinone electronic state is ca. 14 kcal mol^{-1} higher in energy than the copper(II) semiquinone triplet electronic state (Figure 12). With increasing rhombic distortion, the copper(I) quinone electronic state is

dx.doi.org/10.1021/ic200958g |*Inorg. Chem.* 2011, 50, 9816–9825

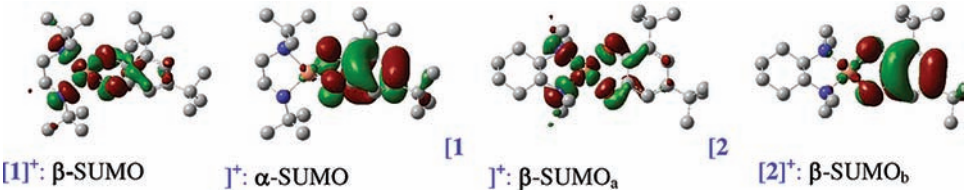

Figure 10. Copper semiquinone SUMO for $[\mathbf{1}]^+$ (left) and $[\mathbf{2}]^+$ (right).

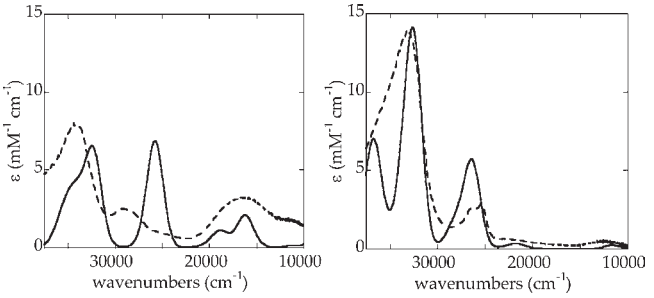

Figure 11. Comparison of the TD-DFT-computed electronic spectra of $[\mathbf{1}]^+$ (left; exp:calc, dashed:solid) and $[\mathbf{2}]^+$ (right; exp:calc dashed:solid) using a 2000 cm^{-1} linewidth.

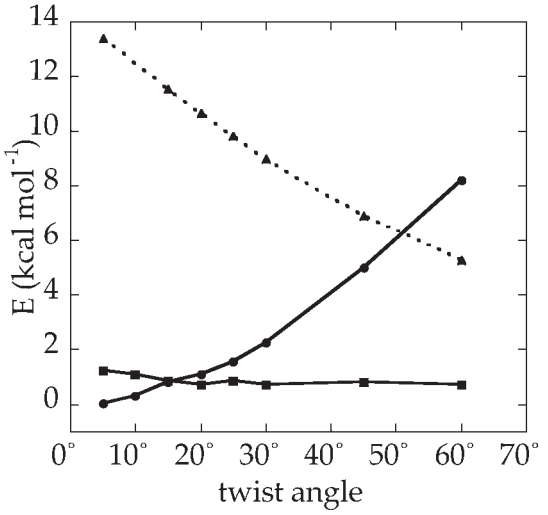

Figure 12. DFT-computed relaxed electronic energy scan of [(ethylenediamine)Cu^{II}-semiquinone]$^+$ (broken-symmetry singlet, squares; triplet, dots) and [(ethylenediamine)Cu^{I}(quinone)]$^+$ (dashed line).[38]

stabilized and becomes energetically favored relative to the triplet state for twists larger than ca. 50°. This is consistent with the preferences of Cu^{I} and Cu^{II} centers for tetrahedral and square-planar geometries, respectively. Notably, the copper(II) semiquinone broken-symmetry state is significantly more stable than the copper(I) quinone state for all rhombically distorted structures.

DISCUSSION

Herein is reported a nontraditional copper(II) semiquinone complex, $[\mathbf{1}]^+$, with a diamagnetic ground state and an intense purple visible absorption band; previously reported copper(II) semiquinone complexes exhibit weak visible absorptions and a

Scheme 2. Twist Angle in $Cu-N_2O_2$ Coordination

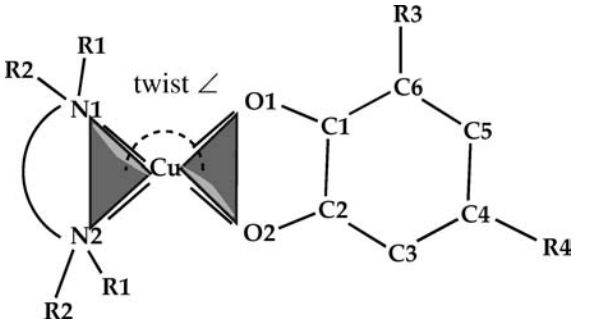

Table 7. Selected TD-DFT-Computed Transitions

	E (cm^{-1}) [f][a]	pre. donor/ acceptor MOs	assignment
$[\mathbf{1}]^+$	25 700 [0.122]	α-HOMO−3 → α-SUMO	intraring semiquinone $\pi-\pi$
	16 200 [0.032]	β-HOMO−3 → β-SUMO	LMCT
$[\mathbf{2}]^+$	27 700 [0.187]	β-HOMO−3 → β-$SUMO_b$	intraring semiquinone $\pi-\pi$

[a] TD-DFT oscillator strength.

ferromagnetic ground state. Comparative characterization of the copper(II) catecholate (**1** and **2**) and copper(II) semiquinone complexes ($[\mathbf{1}]^+$ and $[\mathbf{2}]^+$) provides key insight into the geometric and electronic structural features that lead to these nontraditional magnetic and optical properties of $[\mathbf{1}]^+$. Characterization of $[\mathbf{1}]^+$ was motivated by its postulated presence in the hydroxylation reaction of DBPHO by $^{S}\mathbf{P}^{DBED}$, a faithful spectroscopic and functional model of oxygenated tyrosinase (Figure 1).[18−20]

Copper(II) Semiquinone Description of $[\mathbf{1}]^+$. The copper(II) semiquinone complexes ($[\mathbf{1}]^+$ and $[\mathbf{2}]^+$) in this study were synthesized by the anaerobic reaction of free DBQ with an equimolar mixture of $[Cu^{I}(MeCN)_4]^+$ and the appropriate diamine ligand (Scheme 1). In the DBED case, the diamagnetic complex formed is best described as a copper(II) semiquinone with an antiferromagnetic ground state rather than the other potential diamagnetic electronic descriptions, a copper(I) quinone or a copper(III) catecholate species (Scheme 3).[39] The Cu^{II} oxidation state is consistent with XPS analysis in each case; the Cu $3p_{3/2}$ edge occurs at 933.7 eV in $[\mathbf{1}]^+$ (Figure S5 in the Supporting Information).[9,29] By comparison, the Cu $3p_{3/2}$ edge feature of **1**, a copper(II) catecholate complex, is at 932.9 eV, while that of $[\mathbf{2}]^+$, a paramagnetic semiquinone species, is at 934.1 eV. The 1372 cm^{-1} feature in the intraligand region of the

dx.doi.org/10.1021/ic200958g |Inorg. Chem. 2011, 50, 9816–9825

Scheme 3. Redox Isomers of Copper *o*-Oxolene Complexes

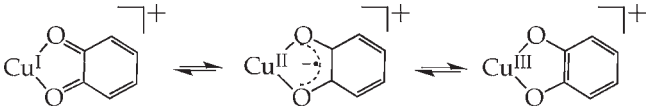

rR spectrum of $[\mathbf{1}]^+$ is diagnostic of C−O/ring deformation modes in metal-bonded semiquinones.[20] The 350 nm optical feature in $[\mathbf{1}]^+$ is also observed in free 3,5-di-*tert*-butylsemiquinone generated electrochemically and attributed to a transition within the semiquinone π system.[23,33]

The semiquinone oxidation state assignment of the ring in $[\mathbf{1}]^+$ is supported by the X-ray crystal structure metrical parameters. The C−O bond distances of ca. 1.35 Å in **1** are consistent with a single bond (i.e., a catecholate ring), and the contracted distances in $[\mathbf{1}]^+$ (ca. 1.27 and 1.29 Å) signify only a partial double-bond character in $[\mathbf{1}]^+$. The two short/four long pattern of the C−C distances in $[\mathbf{1}]^+$ is consistent with a quinoid ring structure.[29] Similar patterns in the bond distances in $[\mathbf{2}]^+$ support its assignment as a copper(II) semiquinone complex. DFT geometry optimizations of the broken-symmetry singlet and triplet electronic state structures of $[\mathbf{1}]^+$ and $[\mathbf{2}]^+$, respectively, also reproduce the quinoid bond pattern (Table 6).

Optical Redox Titrations. The reversible titration of **1** or $[\mathbf{1}]^+$ at room temperature using 1 equiv of Fc^+ and $CoCp_2$ clearly indicates that these complexes are related by a reversible one-electron redox process. The chemical oxidation and reduction of **1** is accompanied by the growth and decay of the 350 and 580 nm optical features, respectively. The 350 nm feature, attributable to charge transfer within the semiquinone π system, is consistent with a ligand-based rather than a metal-based locus of oxidation, yielding a copper(II) semiquinone rather than copper(III) catecholate. Elongation of the average Cu−O bond distances in $[\mathbf{1}]^+$ relative to **1** is also consistent with ligand-based oxidation. On the basis of these results, the −570 mV redox couple versus $Fc^{0/+}$ can be attributed to a catecholate/semiquinone redox transformation.

Intense Purple Chromophore in $[\mathbf{1}]^+$. The visible absorption band that is intense in $[\mathbf{1}]^+$ is much more modest in $[\mathbf{2}]^+$ and other copper(II) semiquinone complexes. DFT computations suggest that this feature is associated with a LMCT originating from a semiquinone π orbital donating into the unoccupied molecular orbital containing significant Cu 3d character. TD-DFT spectra computed for copper(II) semiquinone structures constrained in a planar coordination geometry show a much more attenuated intensity for the LMCT features relative to their twisted counterparts. A rhombic distortion increases the overlap between the donor and acceptor orbitals, leading to an increase in intensity.[40]

Diamagnetism in Copper(II) Semiquinone. Solid-state magnetic susceptibility measurements confirm the diamagnetic and paramagnetic nature of the ground states in $[\mathbf{1}]^+$ and $[\mathbf{2}]^+$, respectively (Figure 8). Samples of $[\mathbf{1}]^+$ exhibit a small paramagnetic susceptibility signal in SQUID measurements, which is attributed to <5% monomeric copper(II) impurity based on a comparison with **1**. In the low-field region of the Brillouin magnetization curve (5−300 K and 0.1−0.5 T), the paramagnetic susceptibilities of **1** and $[\mathbf{2}]^+$ exhibit the expected Curie behavior (linear vs $1/T$) with effective magnetic moments of 1.6 and 2.5 μ_B. These values are consistent with one and two unpaired spins per complex, respectively. Evans' method measurements of bulk solution magnetic susceptibilities of **1**, $[\mathbf{1}]^+$, and $[\mathbf{2}]^+$ are consistent with the same ground-state descriptions as the solid-state results (Table 5).[41,47]

^{1}H NMR characterization of monomeric copper(II) complexes is typically limited because of the comparable relaxation rates of relevant nuclear and electronic spins leading to severely broadened resonances.[37] Indeed, the ^{1}H NMR spectra of the monomeric, doublet copper(II) catecholate complexes **1** and **2** contain only severely broadened resonances. The proton resonances of $[\mathbf{2}]^+$, a triplet, could all be detected, but the resonances are paramagnetically shifted and broadened.[29] By contrast, the diamagnetic ground state of $[\mathbf{1}]^+$ makes it amenable to ^{1}H NMR chracterization; the spectra of $[\mathbf{1}]^+$ contain relatively sharp resonances that shift reversibly with temperature (Figure 8). These resonances are assigned by a combination of variable-temperature and two-dimensional ^{1}H and ^{13}C NMR measurements.[29] The temperature dependence of the chemical shifts is best modeled by the partial population of an excited triplet state, ca. 6.5 kcal mol^{-1} (2300 cm^{-1}) higher than the singlet ground state.[29] This result supports antiferromagnetic coupling between the Cu^{II} and semiquinone radical spins as the origin of diamagnetism in $[\mathbf{1}]^+$.

Influence of the Twist in Geometry. The most striking structural feature of $[\mathbf{1}]^+$ is the 51° rhombic distortion from a planar geometry that distinguishes it from the more planar $[\mathbf{2}]^+$ (14° distortion) and all previously structurally characterized copper(II) semiquinone complexes (Table S2 in the Supporting Information).[12,16,22−24] The τ_4 parameter is a measure of rhombic distortion in four-coordinate complexes; 0 indicates an undistorted planar geometry, and 1 indicates a tetrahedral geometry; the $[\mathbf{1}]^+$ structure is distorted to halfway between a planar geometry and a tetrahedral geometry. Examples of severely tetrahedrally distorted Cu^{II} coordinations are found in the crystal structures of a bis(μ-hydroxo)dicopper(II) complex of DBED and (spartiene)$Cu^{II}Cl_2$.[27,48]

DFT calculations provide insight into the mechanism of electron coupling in $[\mathbf{1}]^+$ and $[\mathbf{2}]^+$. The mechanism of ferromagnetic exchange in planar copper(II) semiquinone complexes due to the orthogonality of the copper and the semiquinone radical has been discussed previously.[42,43,46] The distortion from planar geometry leads to an increase in the overlap between the Cu 3d orbital in the basal plane and the semiquinone π orbitals and, consequently, stabilizes the diamagnetic ground state in $[\mathbf{1}]^+$. DFT calculations on the simplest diamine/quinone system (Figure 12) suggest that the crossover point lies at a twist angle of ca. 20°; with solid-state twist angles of 51° and 14°, the magnetic behavior of $[\mathbf{1}]^+$ and $[\mathbf{2}]^+$, respectively, is consistent with the DFT computations.

Two key experimental observations are as follows: $[\mathbf{2}]^+$ is a planar ferromagnetic complex, and $[\mathbf{1}]^+$ is a rhombically distorted complex with an antiferromagnetic ground state. From these observations, it can be inferred that, for copper(II) semiquinone complexes with diamine ligands with limited steric bulk, a planar coordination with a triplet ground state is energetically preferred. Increasing the steric demands of the diamine ligands leads to a twist in the coordination sphere due to the steric clash between substituents of the ligand and oxygen atoms of the semiquinone. Indeed, the twist angle of the optimized copper(II) semiquinone structures within a series of N,N′-substituted diamines and unsubstituted semiquinone (H, 11°; Me, 20°; ^{i}Pr, 33°; ^{t}Bu, 39°) increases with increasing steric demands (Figure 13). Calculations using the 3,5-di-*tert*-butyl-substituted

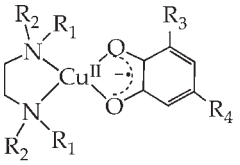

R_1	H	Me	^{i}Pr	^{t}Bu	Me	^{i}Pr	^{t}Bu
R_2	H	H	H	H	H	H	H
R_3	H	H	H	H	^{t}Bu	^{t}Bu	^{t}Bu
R_4	H	H	H	H	^{t}Bu	^{t}Bu	^{t}Bu
twist (°) S = 1	12	20	33	39	22	32	42
S = 0	32	29	42	47	32	44	50
						exp	51

Figure 13. Calculated twist-angle dependence on diamine and ring substituents.

semiquinone ring indicate that the steric clash between the semiquinone and the diamine ligand is of lesser importance in setting the rhombic distortion of the structure.[44]

CONCLUSION

A unique diamagnetic copper(II) semiquinone complex with an intense purple chromophore is fully characterized. The extreme isotropic steric demands of *tert*-butyl substitutents are postulated to be prerequisites for observing these two unique traits. We have established the significant rhombic distortion of the coordination sphere, leading to an overlap between the Cu 3d and semiquinone π systems as the origin of the diamagnetic behavior and the intensity of the purple chromophore. Independent characterization of $[\mathbf{1}]^+$ allows the optical yield of copper(II) semiquinone formed in the hydroxylation reaction with $^{S}\mathbf{P}^{DBED}$ to be estimated at less than 50% of the initial oxidizing equilvalents in $^{S}\mathbf{P}^{DBED}$, a value that correlates with the isolated yield of hydroxylated catechol and quinone products.

Materials and Methods. All solvents and reagents were obtained from commercial sources and used as received unless noted otherwise. See the Supporting Information, including CIF files, for details of X-ray crystal structure data collection and structure solution. Cyclic voltammetry was performed using a BAS CV-40 potentiometer, a silver wire reference electrode, a glassy carbon working electrode, and a platinum disk counter electrode with 0.1 Bu_4NPF_6 solutions in CH_2Cl_2 under N_2 at room temperature and 200 K. Ferrocene was used as an internal standard. X-band EPR spectra were collected with a Bruker EMX spectrometer using an ER041XG microwave bridge and an ER4102ST cavity for experiments conducted at 77 K. UV−vis spectroscopy was performed using a Cary 50 dual-beam spectrophotometer. Variable-temperature (room temperature to 200 K) Evans' method ^{1}H NMR measurements were performed on a Varian Inova 300 MHz instrument in CD_2Cl_2 with tetramethylsilane (TMS) as an internal standard, and diamagnetic corrections were estimated using Pascal's constants. Solvent contraction was accounted for in all variable-temperature studies. Two-dimensional ^{1}H−^{1}H COSY and ^{1}H−^{13}C HSQC NMR experiments were performed on a Mercury 600 MHz instrument in CD_2Cl_2 with TMS as an internal standard at 200 K. Analytical services were provided by Desert Analytics (Tucson, AZ). X-ray photoelectron spectroscopy (XPS) was recorded on a Thermo VG Scientific Model Theta Probe spectrometer using Al Kα radiation (1486.6 eV) operated at 15 kV and 3 mA. The solid sample was dispersed on a silicon substrate, and the C 1s binding energy (284.2 eV) was used to calibrate the binding energy. Solid-state variable-temperature magnetic susceptibility data were collected on a Quantum Design MPMS-XL SQUID. Powdered microcrystalline samples were added to a gel cap and held in place with eicosane (Aldrich). Data were collected in the temperature range 5−300 K and at the field range 0.1−0.5 T. The raw signal was corrected for the diamagnetic signal of the gel cap, eicosane, and the complex (with complex diamagnetic corrections estimated using Pascal's constants). IR data were collected on thin films deposited on NaCl plates from CH_2Cl_2 solutions under an anaerobic atmosphere.

1. A solution of 2,4-di-*tert*-butylquinone (400 mg, 2 mmol, 1 equiv) in dry THF was treated with a freshly activated (treated with acid to remove the copper oxide layer) copper powder (200 mg, 3.2 mmol, 1.6 equiv) under N_2 at room temperature. After 1 h, the color changed to dark blue, DBED (400 mg, 2.3 mmol, 1.1 equiv) was added, and the suspension was stirred for 1 day. The violet solution was filtered and the solvent removed in vacuo to give 0.680 g (75%) of violet crystals. The complex is sparingly soluble even in pentane. An acid quench of **1** in CH_2Cl_2 with excess aqueous 0.1 N HCl and workup yields a 0.05:1 ratio of DBQ and DBCAT, as quantified by ^{1}H NMR spectroscopy. Anal. Found (calcd) for $C_{24}H_{44}CuN_2O_2$ (456.2): C, 62.79 (63.19); H, 10.58 (9.72); N, 6.11 (6.14). IR (thin film, ν [cm^{-1}]): 1256 [ν(C−O/ring)], 1320 [ν(C−O/ring)], 1416, 1435, 1465, 1550, 2960 [ν(C−H)], 3210 [ν(N−H)].

2. A solution of 2,4-di-*tert*-butylquinone (400 mg, 2 mmol, 1 equiv) in dry CH_2Cl_2 was treated with a freshly activated (treated with acid to remove the copper oxide layer) copper powder (200 mg, 3.2 mmol, 1.6 equiv) under N_2 at room temperature. After 1 h, the color changed to dark blue, racemic TMCD (340 mg, 2.0 mmol, 1.0 equiv) was added, and the suspension was stirred overnight. The green solution was filtered to remove excess copper and concentrated to 2 mL, and pentane was added to induce precipitation. The resulting microcrystalline solid was collected by filtration, rinsed with pentane until clear, and dried under N_2 for 4 h to yield 0.250 g (55% yield) of a green solid. X-ray-quality crystals without disorder in the cyclohexyl backbone could not be obtained.

*[**1**]*$^+$. A solution of DBED (0.172 g, 1 mmol) was added to a solution of $[Cu^{I}(CH_3CN)_4]^+PF_6^-$ (0.372 g, 1 mmol) in dry THF and stirred for 5 min under N_2 at room temperature. The clear copper(I) solution was treated with DBQ (0.220 g, 1 mmol) and stirred for 2 h. The intensely colored purple solution was concentrated to 2 mL, and Et_2O was added to induce precipitation. The resulting microcrystalline solid was collected by filtration and rinsed with pentane until the filtrate was clear. The solid was dried under N_2 for 4 h to yield 0.544 g (90% yield) of a purple solid. BF_4^- and SbF_6^- complexes were prepared analogously. X-ray-quality crystals with SbF_6^- counterion were obtained by diffusion of Et_2O into THF solution under N_2 at room temperature. An acid quench of $[\mathbf{1}]^+$ in CH_2Cl_2 with excess aqueous 0.1 N HCl and workup yields a 1:1 ratio of DBQ and DBCAT as quantified by ^{1}H NMR spectroscopy. Anal. Found (calcd) for $C_{24}H_{44}CuN_2O_2SbF_6\cdot 0.5THF$ (727.9): C, 42.60 (42.90); H, 6.45 (6.65); N, 3.83 (3.85). IR (thin film, ν [cm^{-1}]): 757 (SbF_6^-), 1203 [ν(C−O/ring)], 1375 [ν(C−O/ring)], 1475, 1583, 2960 [ν(C−H)], 3255 [ν(N−H)].

*[**2**]*$^+$. The TMCD complex was synthesized in 85% yield following a procedure similar to that of $[\mathbf{1}]^+$. An acid quench of $[\mathbf{2}]^+$ in CH_2Cl_2 with excess aqueous 0.1 N HCl and workup yields a 1:1 ratio of DBQ and DBCAT, as quantified by ^{1}H NMR spectroscopy. IR (thin film, ν [cm^{-1}]): 757 (SbF_6^-), 860, 1008, 1433, 1463, 1530, 1578, 2960 [ν(C−H)].

dx.doi.org/10.1021/ic200958g |*Inorg. Chem.* 2011, 50, 9816–9825

Theoretical Details. DFT calculations were performed using *Gaussian 03* and *Gaussian 09* programs with the B3LYP functional in vacuum. See the Supporting Information for the full Gaussian reference.[29] A double-ζ Pople basis set [6-31g(d) on all atoms] was used for geometry optimizations and frequency calculations and a triple-ζ Pople basis set [6-311+g(d) on Cu, O, and N atoms and 6-31g(d) on all other atoms] was used for single-point and time-dependent DFT (TD-DFT) calculations. The copper(I) quinone, antiferromagnetic copper(II) semiquinone, and ferromagnetic copper(II) semiquinone electronic states were modeled as the spin-restricted singlet, broken-symmetry singlet, and spin-unrestricted triplet single-determinant solutions, respectively. All broken-symmetry solutions yielded nonzero $\langle S^2 \rangle$ values, and the single-point energies were corrected for spin contamination using the summation method.[45]

■ ASSOCIATED CONTENT

Supporting Information. X-ray crystallographic data in CIF format, full citation for ref [1], selected crystallographic data, selected X-ray crystal structure and DFT-computed metrical parameters, cyclic voltammograms, EPR, UV−vis, and XPS spectra, redox titrations, ^{1}H NMR spectra, and an ORTEP representation. This material is available free of charge via the Internet at http://pubs.acs.org.

■ AUTHOR INFORMATION

Corresponding Author
*E-mail: stack@stanford.edu.

■ ACKNOWLEDGMENT

We thank Prof. Edward I. Solomon for use of the EPR instrument, Prof. Ian Fisher for use of the MPMS SQUID magnetometer, and Prof. Hongjie Dai for use of the Raman instrument. The single-crystal X-ray diffraction data in this work were recorded on an instrument supported by the National Science Foundation, Major Research Instrumentation Program, under Grant CHE-0521569.

■ REFERENCES

(1) Hendrickson, D. N.; Pierpont, C. G. *Top. Curr. Chem.* **2004**, *234*, 63.
(2) Dei, A.; Gatteschi, D.; Sangregorio, C.; Sorace, L. *Acc. Chem. Res.* **2004**, *37*, 827.
(3) Gatteschi, D.; Bogani, L.; Cornia, A.; Mannini, M.; Sorace, L.; Sessoli, R. *Solid State Sci.* **2008**, *10*, 1701.
(4) Gatteschi, D. *Nat. Mater.* **2007**, *6*, 471.
(5) Zarkesh, R. A.; Ziller, J. W.; Heyduk, A. F. *Angew. Chem., Int. Ed.* **2008**, *47*, 4715.
(6) Blackmore, K. J.; Lal, N.; Ziller, J. W.; Heyduk, A. F. *J. Am. Chem. Soc.* **2008**, *130*, 2728.
(7) Kaim, W.; Schwederski, B. *Pure Appl. Chem.* **2004**, *76*, 351.
(8) Ye, S.; Sarkar, B.; Lissner, F.; Schleid, T.; van Slageren, J.; Fiedler, J.; Kaim, W. *Angew. Chem., Int. Ed.* **2005**, *44*, 2103.
(9) Storr, T.; Verma, P.; Pratt, R. C.; Wasinger, E. C.; Shimazaki, Y.; Stack, T. D. P. *J. Am. Chem. Soc.* **2008**, *130*, 15448.
(10) Pratt, R. C.; Stack, T. D. P. *Inorg. Chem.* **2005**, *44*, 2367.
(11) Kodera, M.; Kawata, T.; Kano, K.; Tachi, Y.; Itoh, S.; Kojo, S. *Bull. Chem. Soc. Jpn.* **2003**, *76*, 1957.
(12) Berreau, L. M.; Mahapatra, S.; Halfen, J. A.; Houser, R. P.; Young, V. G.; Tolman, W. B. *Angew. Chem., Int. Ed.* **1999**, *38*, 207.
(13) Speier, G.; Tyeklár, Z.; Toth, P.; Speier, E.; Tisza, S.; Rockenbauer, A.; Whalen, A. M.; Alkire, N.; Pierpont, C. G. *Inorg. Chem.* **2001**, *40*, 5653.
(14) Speier, G.; Csihony, J.; Whalen, A. M.; Pierpont, C. G. *Inorg. Chem.* **1996**, *35*, 3519.
(15) Dei, A.; Gatteschi, D.; Pardi, L. *Inorg. Chem.* **1993**, *32*, 1389.
(16) Dei, A.; Gatteschi, D.; Pardi, L.; Barra, A. L.; Brunel, L. C. *Chem. Phys. Lett.* **1990**, *175*, 589.
(17) Ye, S. F.; Sarkar, B.; Niemeyer, M.; Kaim, W. *Eur. J. Inorg. Chem.* **2005**, 4735.
(18) Mirica, L. M.; Vance, M.; Jackson Rudd, D.; Hedman, B.; Hodgson, K. O.; Solomon, E. I.; Stack, T. D. P. *Science* **2005**, *308*, 1890.
(19) Mirica, L. M.; Rudd, D. J.; Vance, M. A.; Solomon, E. I.; Hodgson, K. O.; Hedman, B.; Stack, T. D. P. *J. Am. Chem. Soc.* **2006**, *128*, 2654.
(20) Holt, B. T. O.; Vance, M. A.; Mirica, L. M.; Heppner, D. E.; Stack, T. D. P.; Solomon, E. I. *J. Am. Chem. Soc.* **2009**, *131*, 6421.
(21) Company, A.; Palavicini, S.; Garcia-Bosch, I.; Mas-Balleste, R.; Que, L.; Rybak-Akimova, E. V.; Casella, L.; Ribas, X.; Costas, M. *Chem.—Eur. J.* **2008**, *14*, 3535.
(22) Ruf, M.; Noll, B. C.; Groner, M. D.; Yee, G. T.; Pierpont, C. G. *Inorg. Chem.* **1997**, *36*, 4860.
(23) Rall, J.; Wanner, M.; Albrecht, M.; Hornung, F. M.; Kaim, W. *Chem.—Eur. J.* **1999**, *5*, 2802.
(24) Thompson, J. S.; Calabrese, J. C. *Inorg. Chem.* **1985**, *24*, 3167.
(25) Thompson, J. S.; Calabrese, J. C. *J. Am. Chem. Soc.* **1986**, *108*, 1903.
(26) Details of the X-ray crystal structure analysis are provided in the Supporting Information.
(27) Yoon, J.; Mirica, L. M.; Stack, T. D. P.; Solomon, E. I. *J. Am. Chem. Soc.* **2004**, *126*, 12586.
(28) Yang, L.; Powell, D. R.; Houser, R. P. *Dalton Trans.* **2007**, 955.
(29) See the Supporting Information.
(30) Hoffmann, S. K.; Goslar, J. *J. Solid State Chem.* **1982**, *44*, 343.
(31) Peisach, J.; Blumberg, W. E. *Arch. Biochem. Biophys.* **1974**, *165*, 691.
(32) Stoll, S.; Schweiger, A. *J. Magn. Reson.* **2006**, *178*, 42.
(33) Jovanovic, S. V.; Konya, K.; Scaiano, J. C. *Can. J. Chem.* **1995**, *73*, 1803.
(34) Using a 300 MHz ^{1}H NMR spectrometer (7.05 T).
(35) Solomon, E. I.; Lever, A. B. P. *Inorganic electronic structure and spectroscopy*, 3rd ed.; Wiley: New York, 1999.
(36) Tepper, A. W. J. W.; Bubacco, L.; Canters, G. W. *Chem.—Eur. J.* **2006**, *12*, 7668.
(37) Holz, R. C.; Brink, J. M. *Inorg. Chem.* **1994**, *33*, 4609.
(38) See the Theoretical Methods section for details.
(39) Only a single example of an isolated O,O′-coordinating *o*-quinone ligand that complexes with copper(I) without reduction has been reported [copper(I) phenanthroquinone]. However, stable copper(I) complexes with *o*-quinone monoimine and *o*-quinone diimine ligands have been reported.Roy, S.; Sarkar, B.; Bubrin, D.; Niemeyer, M.; Zalis, S.; Lahiri, G. K.; Kaim, W. *J. Am. Chem. Soc.* **2008**, *130*, 15230 (ref 1).
(40) The extinction coefficient of pure $[\mathbf{1}]^+$ allows its yield in the hydroxylation reaction with $^{S}\mathbf{P}^{DBED}$ to be estimated at <50% of the expected stoichiometric value, which correlates with the yield of the hydroxylated catechol and quinone products recovered.
(41) It should be noted that solid and solution magnetic suseptibilities are measured under different but complimentary conditions: 5−300 K and 0.1−0.5 T for the solid state and 200−300 K and 7.05 T (300 MHz ^{1}H NMR) for the solution. In addition, lattice constraints on structural rearrangements in the microcrystalline solid-state samples are not relevant in solution samples. Consequently, qualitative rather than quantitative consistency between the solid and solution measurements is expected and observed.
(42) Dei, A.; Gatteschi, D.; Pardi, L.; Russo, U. *Inorg. Chem.* **1991**, *30*, 2589.
(43) Pierpont, C. G.; Attia, A. S. *Collect. Czech. Chem. Commun.* **2001**, *66*, 33.

(44) The preference for a tetrahedral geometry for a Cu^{I} center and a planar geometry for a Cu^{II} center is proposed as a possible influence on redox isomerism in copper(II) catecholate/copper(I) semiquinone complexes. Interestingly, a similar shift in the charge distribution from copper(II) semiquinone to copper(I) quinone does not result from a significant twist in $[\mathbf{1}]^{+}$, likely because of the compensating electron donation from the aliphatic nitrogen ligands that stabilize the higher oxidation state. DFT calculations predict that the copper(I) quinone electronic state is significantly destabilized relative to the copper(II) semiquinone antiferromagnetic electronic state.

(45) Cramer, C. J.; Wloch, M.; Piecuch, P.; Puzzarini, C.; Gagliardi, L. *J. Phys. Chem. A* **2006**, *110*, 1991.

(46) Kahn, O.; Prins, R.; Reedijk, J.; Thompson, J. S. *Inorg. Chem.* **1987**, *26*, 3557.

(47) DFT computed singlet−triplet energy gaps are functional-dependent: the hybrid B3LYP and the pure BLYP functionals predict the broken-symmetry state to be more stable for $[\mathbf{1}]^{+}$ by 1900 and 2500 cm^{-1}, respectively. The value estimated from ^{1}H NMR measurements is ca. 2300 cm^{-1}.

(48) Funahashi, Y.; Nakaya, K.; Hirota, S.; Yamauchi, O. *Chem. Lett.* **2000**, 1172.